


## Theory of the Supercurrent Diode Effect in Rashba Superconductors with Arbitrary Disorder

S. Ilić<sup>1</sup> and F. S. Bergeret<sup>1,2</sup>

<sup>1</sup>*Centro de Física de Materiales (CFM-MPC), Centro Mixto CSIC-UPV/EHU, Manuel de Lardizabal 5, E-20018 San Sebastián, Spain*

<sup>2</sup>*Donostia International Physics Center (DIPC), Manuel de Lardizabal 4, E-20018 San Sebastián, Spain*

 (Received 26 January 2022; revised 22 March 2022; accepted 31 March 2022; published 27 April 2022)

We calculate the nonreciprocal critical current and quantify the supercurrent diode effect in two-dimensional Rashba superconductors with arbitrary disorder, using the quasiclassical Eilenberger equation. The nonreciprocity is caused by the helical superconducting state, which appears when both inversion and time-reversal symmetries are broken. In the absence of disorder, we find a very strong diode effect, with the nonreciprocity exceeding 40% at optimal temperatures, magnetic fields, and spin-orbit coupling. We establish that the effect persists even in the presence of strong disorder. We show that the sign of the diode effect changes as magnetic field and disorder are increased, reflecting the changes in the nature of the helical state.

DOI: [10.1103/PhysRevLett.128.177001](https://doi.org/10.1103/PhysRevLett.128.177001)

*Introduction.*—The interplay between superconductivity, spin-orbit coupling (SOC), and a Zeeman field leads to a variety of magnetoelectric effects widely studied in the past years [1–12]. One of these effects is a nonreciprocal charge transport due to the breaking of time-reversal and inversion symmetries [13–24]. Originally this effect was studied in the resistive regime, when  $T \gtrsim T_c$ , where superconducting fluctuations play a crucial role [14,15]. More recently, it has been shown that nonreciprocity also manifests in the supercurrent in noncentrosymmetric superconducting structures and in Josephson junctions [16–18,20–23,25]. Specifically, the critical current depends on the direction of the current flow, and hence such systems are being suggested as superconducting diodes with potential applications in low-power logic circuits.

The nonreciprocity of the critical current can be quantified by the superconducting diode quality parameter

$$\eta = (j_c^+ - |j_c^-|)/(j_c^+ + |j_c^-|), \quad (1)$$

where  $j_c^\pm$  are the critical currents in opposite directions. It has been shown in Refs. [20–22] that  $\eta$  is finite in noncentrosymmetric superconducting systems in the presence of a magnetic field. Namely, the breaking of time-reversal and inversion symmetries in such systems allows for a formation of the helical superconducting phase, with the order parameter modulated in the direction transverse to the field:  $\Delta(\mathbf{r}) = \Delta e^{i\mathbf{q}_0 \cdot \mathbf{r}}$ . Therefore, Cooper pairs have a finite momentum  $\mathbf{q}_0$ . Consequently, the depairing effect of supercurrents flowing parallel and antiparallel to  $\mathbf{q}_0$  is different, leading to a direction-dependent critical current.

Importantly, the above-mentioned theoretical works assume ideally pure superconducting structures and

disregard the effect of disorder. However, the latter is unavoidable in realistic structures, and therefore it is important to understand how it affects the supercurrent diode effect. Moreover, understanding the role of disorder will enable one to design devices based on a combination of conventional materials.

In this Letter, we establish a microscopic theory of the supercurrent diode effect in disordered two-dimensional Rashba superconductors. As a base of our study, we use the quasiclassical equations for superconductors with strong Rashba SOC from Ref. [26], which give a full description of the helical superconducting phase at arbitrary temperature, magnetic field, and disorder. These equations provide a straightforward framework to discuss the diode effect, within which we readily reproduce previous results of numerical simulations in the ballistic limit [22], and generalize them for arbitrary disorder. Moreover, we correct previous works based on the phenomenological Ginzburg-Landau (GL) theory [20,21], which overestimate the diode effect at weak fields and close to critical temperature.

Our results elucidate the mechanisms leading to the diode effect, and show how it evolves in the full range of all relevant system parameters: SOC, magnetic field, temperature, and disorder. Namely, the effect stems from the competition between two helical bands in a Rashba superconductor, which prefer opposite modulation vectors of the superconducting order parameter when magnetic field is applied. Both magnetic field and SOC are required for the diode effect; however, if either is too strong, the band competition ceases as one helical band begins to dominate, leading to the suppression of the effect. This means that a substantial  $\eta$  exists only for some optimal magnetic field and SOC. Disorder further complicates this picture, as it

introduces mixing of the two helical bands. We discuss optimal parameter regimes where the effect is strongest (exceeding  $\eta = 40\%$  in the ballistic case). We establish that the effect persists at strong disorder, meaning that it can be realized even in disordered materials and hybrid systems. Moreover, we show that the sign  $\eta$  changes as the magnetic field is increased [22], and also by increasing the disorder. The change of sign of  $\eta$  can be related to the change of nature of the helical phase.

*Quasiclassical theory.*—The quasiclassical Eilenberger equation for a two-dimensional disordered Rashba superconductor with strong SOC, in the basis of two helical bands denoted with the index  $\lambda = \pm 1$ , is [26]

$$v\mathbf{n} \cdot \partial_\lambda \check{g}_\lambda + [(\omega + i\check{\Delta})\tau_z + \sigma_\lambda^{\text{imp}}, \check{g}_\lambda] = 0. \quad (2)$$

Here  $\check{g}_\lambda$  is the quasiclassical Green's function in the Matsubara representation, which is a matrix in Nambu space spanned by the Pauli matrices  $\tau_{x,y,z}$ .  $\omega = 2\pi T(n + \frac{1}{2})$  is the Matsubara frequency, with  $T$  being the temperature. Importantly, the two bands have the same Fermi velocity  $v = \sqrt{2\mu/m + \alpha^2}$ , but different densities of states,  $\nu_\lambda = \nu(1 - \lambda\alpha/v)$ . Here,  $\mu$  is the chemical potential,  $m$  is the effective electron mass,  $\alpha$  is the velocity associated with Rashba SOC, and  $\nu = m/(2\pi)$ . We introduced the derivative  $\partial_\lambda = \nabla + i(\lambda/v)(\mathbf{h} \times \mathbf{z})[\tau_z, \cdot]$ ,  $\mathbf{h}$  is the in-plane magnetic field, and  $\mathbf{n} = \mathbf{p}/p_F = (n_x, n_y)$  describes the direction of the momentum at the Fermi level. The superconductivity is accounted for by the term  $\check{\Delta} = \Delta(\mathbf{r})\tau_+ + \Delta^*(\mathbf{r})\tau_-$ , with  $\tau_\pm = \frac{1}{2}(\tau_x \pm i\tau_y)$ , where  $\Delta$  is the superconducting order parameter. The normalization condition is satisfied for each helical band:  $\check{g}_\lambda^2 = 1$ .

Disorder is described by the self-energy  $\sigma_\lambda^{\text{imp}}$  given as

$$\sigma_\lambda^{\text{imp}} = \sum_{\lambda'} (4\tau_{\lambda'})^{-1} [\langle \check{g}_{\lambda'} \rangle + \lambda\lambda' \mathbf{n} \cdot \langle \mathbf{n} \check{g}_{\lambda'} \rangle]. \quad (3)$$

Here,  $\langle \dots \rangle$  denotes averaging over  $\mathbf{n}$ , and we introduced  $\tau_\lambda^{-1} = [1 - \lambda(\alpha/v)]\tau^{-1}$ , where  $\tau^{-1}$  is the disorder scattering rate. Note that  $\sigma_\lambda^{\text{imp}}$  stems from a simple scalar disorder potential, which acquires the form shown in Eq. (3) upon projection to the helical basis [26].

Equation (2) is valid for very strong SOC, so that it is larger than all other energy scales relevant for superconductivity except the chemical potential:  $\mu \gtrsim \alpha p_F \gg \Delta, h, \tau^{-1}$ . Under these conditions, interband pairing can be neglected, and Cooper pairs can be taken to be formed in each helical band separately. In the absence of disorder, the two bands are decoupled, while sharing the same superconducting gap  $\Delta$ . Any finite disorder mixes the two bands.

To proceed, we assume that the superconducting phase varies only along the  $x$  direction, and that the Zeeman field is applied along the  $y$  direction:  $\mathbf{h} = (0, h)$ ; see Fig. 1(a). We take that  $\Delta(x) = \Delta e^{iqx}$  [27], where  $q = q_0 + \delta q$  is the

phase gradient which contains two contributions: intrinsic modulation of the helical phase  $q_0$ , and an additional phase gradient caused by passing the supercurrent  $\delta q$ . Then, we write the Green's function as  $\check{g}_\lambda(x) = g_\lambda \tau_z + \tilde{f}_\lambda(x) \tau_+ + \tilde{f}_\lambda^*(x) \tau_-$ , and we look for the solution in the form  $\tilde{f}_\lambda(x) = -if_\lambda e^{iqx}$ . The normalization condition gives  $g_\lambda^2 = 1 - f_\lambda^2$ . With this parametrization,  $\Delta$ ,  $f_\lambda$ , and  $g_\lambda$  are real quantities. The Eilenberger equation then reduces to the following scalar equation

$$f_\lambda(2\omega + in_x \rho_\lambda) = 2\Delta g_\lambda + \sum_{\lambda'} (2\tau_{\lambda'})^{-1} [g_\lambda \langle f_{\lambda'} \rangle - f_\lambda \langle g_{\lambda'} \rangle + \lambda\lambda' n_x (g_\lambda \langle n_x f_{\lambda'} \rangle - f_\lambda \langle n_x g_{\lambda'} \rangle)]. \quad (4)$$

Here, we introduced  $\rho_\lambda = qv + 2\lambda h$ .

The order parameter is determined self-consistently as

$$\Delta \ln \frac{T}{T_c} + \pi T \sum_{\omega > 0} \sum_{\lambda} \left[ \frac{\Delta}{\omega} - \left( 1 - \lambda \frac{\alpha}{v} \right) \langle f_\lambda \rangle \right] = 0. \quad (5)$$

Here,  $T_c$  is the critical temperature of the superconductor in the absence of a magnetic field. Finally, the current along the  $x$  direction is given as

$$j = -4\pi T i v \sum_{\omega > 0} \sum_{\lambda} \nu_\lambda \langle n_x g_\lambda \rangle. \quad (6)$$

Importantly,  $j(q_0) = 0$ —there should be no supercurrent flowing in the equilibrium [28].

Eqs. (4)–(6) are a starting point for studying the diode effect. First,  $\Delta(q)$  should be calculated self-consistently from Eqs. (4) and (5) for all values of  $q$  where  $\Delta$  is finite. Next, using  $\Delta(q)$  obtained this way, one should calculate  $j(q)$  from Eq. (6). Then, the critical currents in the two directions are determined as  $j_c^+ = \max[j(q)]$  and  $j_c^- = \min[j(q)]$ . Finally, the diode quality factor  $\eta$  is obtained by replacing  $j_c^\pm$  obtained this way in Eq. (1).

*Ballistic case.*—Before discussing the diode effect, it is first useful to understand the evolution of the helical phase in magnetic fields. The two helical bands with  $\lambda = \pm 1$  prefer opposite modulation vectors:  $q_0^\lambda v = -2\lambda h$ . At low magnetic fields, both bands contribute to helical superconductivity, which yields a modulation vector  $q_0 v \approx 2(\alpha/v)h$ . This regime is known as a long-wavelength or “weak” helical phase [28]. As the magnetic field is increased, the band with the higher density of states begins to dominate, whereas the contribution from the other band is suppressed. Therefore, at a strong-enough field only one band contributes, and the modulation vector becomes  $q_0 v \approx 2h$ . This is a short wavelength or “strong” helical phase” [28]. The crossover from a “weak” to “strong” phase is illustrated in Fig. 1(b). Note that if the two bands have similar densities of states, at  $\alpha/v \ll 1$ , the so-called stripe phase might stabilize instead of the strong helical

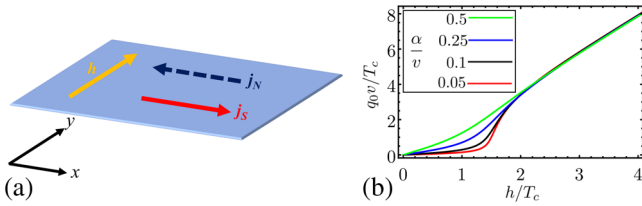


FIG. 1. (a) Schematic representation of the setup considered in this work. The current flows in the  $x$  direction, and the Zeeman field lies along the  $y$  direction. If the conditions for the diode effect are satisfied, the supercurrent  $j_S$  can flow in one direction, whereas only a regular Ohmic current  $j_N$  can flow in the other. (b) Helical modulation vector  $q_0$  calculated in the vicinity of the upper critical field  $h_{c2}$ , as a function of magnetic field, for different strengths of spin-orbit coupling. At low fields  $q_0 \approx 2(\alpha/v)h$  (“weak helical phase”), whereas at high fields  $q_0 \approx 2h$  (“strong helical phase”).

phase at high fields. The stripe phase is beyond the scope of the present work (see also the footnote in Ref. [27]).

In the absence of disorder, the two helical bands are decoupled, and we readily find the solution of the Eilenberger equation [Eq. (4)] as  $f_\lambda = 2\Delta/\mathcal{A}$  and  $g_\lambda = (2\omega + in_x\rho_\lambda)/\mathcal{A}$ , where  $\mathcal{A} = \sqrt{(2\omega + in_x\rho_\lambda)^2 + 4\Delta^2}$ . The Fermi surface averages that enter Eqs. (5) and (6) can be found analytically (see the Supplemental Material [30]). The critical current and the diode quality factor are then readily calculated following the procedure described below Eq. (6). Several examples of the self-consistent calculation of  $\Delta(q)$ ,  $j(q)$ , and  $\eta$  are shown in Fig. 2.

The upper left panel of Fig. 2 shows the situation with  $h = 0$  and no helical phase. A phase gradient due to the supercurrent introduces depairing, and ultimately leads to a phase transition to the normal state. The upper right panel of Fig. 2 depicts a situation where  $h$  is sufficiently low so that the superconductor is in the “weak” helical state, whereas two lower panels depict a situation with the “strong” helical state. In these three panels, the current has a zero at  $q = q_0$  due to the intrinsic modulation of the helical phase, and all three show nonreciprocity of the critical current. The shape of  $\Delta(q)$  and  $j(q)$  in the “weak” and “strong” state is markedly different, leading to the different behavior of the diode effect. Namely, the effect is negative in the “weak” state ( $j_c^+ < |j_c^-|$ ,  $\eta < 0$ ) and positive in the “strong” state ( $j_c^+ > |j_c^-|$ ,  $\eta > 0$ ).

In Fig. 3, we plot the diode quality factor  $\eta$  for every point in the  $h - T$  phase diagram for different strengths of SOC. The black curve in the plots corresponds to the upper critical field  $h_{c2}$ . At temperatures close to  $T_c$ , the diode effect vanishes up to linear order in  $h$ . We demonstrate this analytically using the GL theory in the Supplementary Material [30]. This result is in contrast with Refs. [20] and [21], which do not take into account all relevant terms in the  $q$  expansion of the GL free energy, and consequently find a finite effect in this regime.

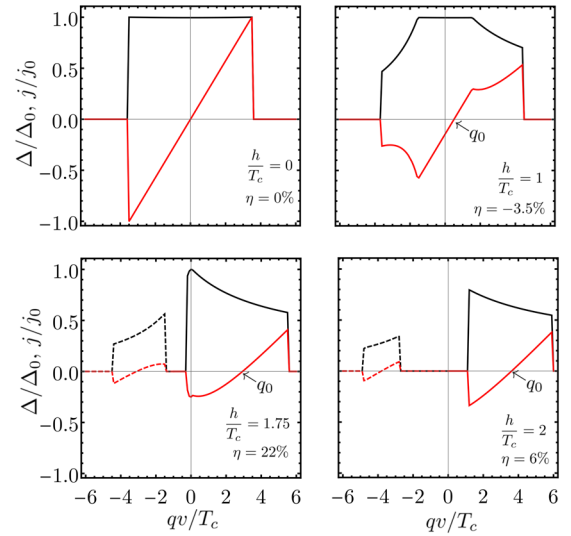


FIG. 2. Superconducting gap (in black) and the supercurrent (in red), calculated self-consistently from Eqs. (5) and (6), respectively. Both quantities are plotted as a function of the phase gradient, for different values of the magnetic field. We normalize the curves with  $\Delta_0$  and  $j_0$ , which are the values of the superconducting gap and the critical current at  $T = h = 0$ . We set  $\alpha/v = 0.25$  and  $T = 0.01T_c$ . Note that at high fields (two lower panels), the self-consistency condition yields two solutions for  $\Delta(q)$ . The solution centered around  $q_0(-q_0)$ , plotted with a full (dashed) line, predominantly comes from the helical band with a higher (lower) density of states. The solution around  $q_0$  is more stable (it minimizes the free energy [29]), and it is the only one relevant for our calculation.

Figure 3 clearly illustrates the two regimes of the diode effect, driven by the “weak” and “strong” helical phases, depicted with orange and purple colors, respectively. These results are in good qualitative agreement with the numerical

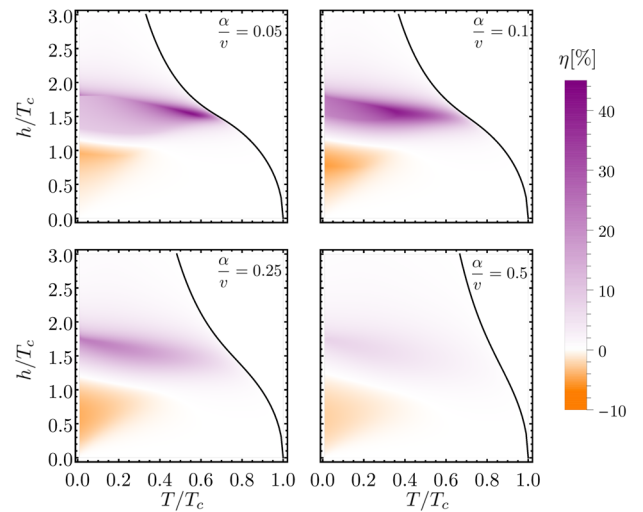


FIG. 3. Diode quality factor  $\eta$  for a ballistic superconductor, calculated for every point in the  $h - T$  phase diagram at different strengths of spin-orbit coupling.

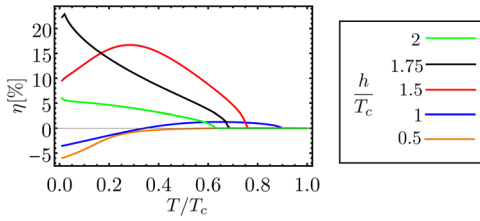


FIG. 4. Diode quality factor as a function of temperature, for different values of the magnetic field, at  $\alpha/v = 0.25$ .

study of Ref. [22]. Figure 3 also showcases that the competition of two helical bands is a crucial ingredient for the diode effect. Namely, if one helical band becomes dominant, while the other one is fully suppressed, the diode effect disappears. One of the ways this can happen is by increasing the magnetic field—after the crossover to the “strong” phase, one band dominates. Another way is by increasing spin-orbit coupling—at large values of  $\alpha/v$ , one band will have a much larger density of states than the other. In fact, at  $\alpha/v = 1$ , only one helical band exists, and the diode effect disappears. Therefore, too large SOC and too large magnetic field both lead to the suppression of the diode effect, as illustrated in Fig. 3.

Note that the coefficient  $\eta$  can have nonmonotonic dependence on the temperature at some fixed magnetic field, as shown in Fig. 4. This can be explained by noticing that the diode effect is strongest close to the field  $h^*$  at which the crossover between the “weak” and “strong” helical phase happens, combined with the fact that  $h^*$  slightly reduces by increasing the temperature. Similar nonmonotonic behavior of  $\eta(T)$  was measured in a recent experiment in a few-layer NbSe<sub>2</sub> [23].

*Systems with disorder.*—As established in the previous discussion in the ballistic limit, the competition between two helical bands upon applying the magnetic field is the driving force behind the diode effect. Very strong disorder mixes the bands, and therefore it suppresses this competition and the diode effect. By increasing disorder, the “strong” helical phase gets suppressed, and for  $\alpha p_F \gg \tau^{-1} \gg \Delta, h$ , only the “weak” phase exists in the whole phase diagram, with the modulation vector  $q_0 = 4ah/(\alpha^2 + v^2)$ . This is illustrated in Fig. 5, where we plot  $q_0$

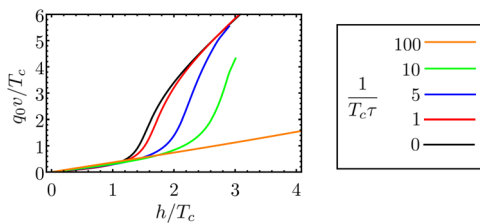


FIG. 5. Helical modulation vector  $q_0$  calculated in the vicinity of  $h_{c2}$ , as a function of magnetic field, for different strengths of disorder. We set  $\alpha/v = 0.1$ . At strong disorder,  $\tau^{-1} \gg \Delta, h$ , we have  $q_0 \approx 4ah/(\alpha^2 + v^2)$ .

for different values of disorder. In the following discussion, we explore the crossover from the strong diode effect in the ballistic case, to its vanishing at sufficiently strong disorder.

We examine the diode effect at arbitrary disorder in the GL regime, close to the phase transition to the normal state. This approach is valid for any  $T$ , as long as  $h$  is sufficiently strong so that the  $\Delta \ll T$ . In order to construct the GL free energy, we solve the Eilenberger equation [Eq. (4)] close to the phase transition. We may expand  $f_\lambda$  up to third order in  $\Delta$ :  $f_\lambda \approx f_\lambda^{(1)} + f_\lambda^{(3)}$ , and  $g_\lambda = \sqrt{1 - f_\lambda^2} \approx 1 - \frac{1}{2}(f_\lambda^{(1)})^2$ . The GL free energy is then

$$F_q = \alpha_q \Delta^2 + \beta_q / 2\Delta^4 \quad (7)$$

where  $\alpha_q = \nu \ln(T/T_c) + 2\pi T \sum_{\omega>0} [(\nu/\omega) - (1/2\Delta) \times \sum_\lambda \nu_\lambda \langle f_\lambda^{(1)} \rangle]$  and  $\beta_q = -2\pi T \sum_{\omega>0} \sum_\lambda (1/2\Delta^3) \nu_\lambda \langle f_\lambda^{(3)} \rangle$  (see Sec. S2 in the Supplemental Material [30]). The order parameter is determined by minimizing the free energy with respect to  $\Delta$ , which gives  $\Delta^2 = -\alpha_q/\beta_q$ . From here, we find the optimal free energy  $F_q^{\text{opt}} = -\alpha_q^2/(2\beta_q)$ . Finally, the current is given as

$$j = 2 \frac{\partial F_q^{\text{opt}}}{\partial q}. \quad (8)$$

Figure 6 shows the values of  $\eta$  at different values of disorder calculated from Eq. (8). The upper left panel corresponds to the ballistic case, and agrees with the results of Fig. 3 obtained from the full self-consistent calculation. Notably, the diode effect qualitatively changes behavior as disorder is increased—it goes from positive to negative. This can be understood as a consequence of the crossover

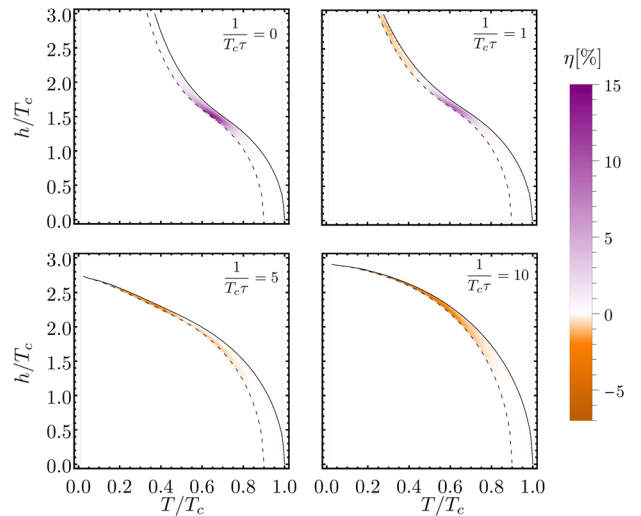


FIG. 6. Diode quality factor in the disordered case, calculated in the GL regime at different strengths of disorder at  $\alpha/v = 0.1$ . The full black line is the phase transition line  $h_{c2}(T)$ , whereas at the dashed line the condition  $\Delta(T) = T$  is satisfied. Between the two lines  $T > \Delta$  holds—this is the region of validity of the GL theory.

from the “strong” to the “weak” helical phase as disorder is increased, which correspond to  $\eta > 0$  and  $\eta < 0$ , respectively, as established previously. The diode effect at  $\tau^{-1} = 10T_c$  reaches a sizeable value of  $\eta \approx -7\%$ . Further increasing disorder ( $\tau^{-1} > 10T_c$ ) leads to a qualitatively similar picture as in the lower right panel of Fig. 6, but with smaller  $\eta$ . In the Supplemental Material [30], we present an analysis of  $\eta$  in a broader disorder range. For example, we find  $\eta$  as large as  $\sim -0.25\%$  at  $\tau^{-1} = 100T_c$ . Note that the results obtained within the GL theory are only a lower bound of the effect, which likely reaches higher values beyond the GL regime.

*Conclusion.*—In summary, based on quasiclassical formalism, we establish a theory of the diode effect in Rashba superconductors with arbitrary disorder. In the ballistic limit, we explore the whole phase diagram of helical superconductivity, and identify the conditions that maximize the diode effect. In the presence of disorder, we identify a new regime of the diode effect, which is qualitatively different from the ballistic limit, and show that a substantial diode effect exists even at strong disorder. Moreover, we show that the sign of the quality factor  $\eta$  is related to the nature of the helical state:  $\eta > 0$  in the “strong” state, and  $\eta < 0$  in the “weak” state. A possible device to experimentally study the effect is a 2D superconductor with strong SOC in a heterostructure with a ferromagnetic insulator such as EuS [31–33], which induces a sizeable exchange field in the superconductor (a few Tesla) necessary to obtain a large diode effect. Moreover, such a device is compatible with applications in superconducting electronics and spintronics, as it does not require applying external magnetic fields.

We thank Manuel Houzet for useful discussions. This work was supported by European Unions Horizon 2020 Research and Innovation Framework Programme under Grant No. 800923 (SUPERTED), and the Spanish Ministerio de Ciencia e Innovacion (MICINN) through Project No. PID2020–114252 GB-I00 (SPIRIT). F. S. B. acknowledges financial support by the A. v. Humboldt Foundation.

---

[1] D. Szombati, S. Nadj-Perge, D. Car, S. Plissard, E. Bakkers, and L. Kouwenhoven, *Nat. Phys.* **12**, 568 (2016).  
 [2] A. Assouline, C. Feuillet-Palma, N. Bergeal, T. Zhang, A. Mottaghizadeh, A. Zimmers, E. Lhuillier, M. Eddrie, P. Atkinson, M. Aprili, and H. Aubin, *Nat. Commun.* **10**, 126 (2019).  
 [3] W. Mayer, M. C. Dartiaillh, J. Yuan, K. S. Wickramasinghe, E. Rossi, and J. Shabani, *Nat. Commun.* **11**, 212 (2020).  
 [4] E. Strambini, A. Iorio, O. Durante, R. Citro, C. Sanz-Fernández, C. Guarcello, I. V. Tokatly, A. Braggio, M. Rocci, N. Ligato *et al.*, *Nat. Nanotechnol.* **15**, 656 (2020).  
 [5] V. M. Edelstein, *Phys. Rev. Lett.* **75**, 2004 (1995).

[6] V. M. Edelstein, *Phys. Rev. B* **72**, 172501 (2005).  
 [7] A. Buzdin, *Phys. Rev. Lett.* **101**, 107005 (2008).  
 [8] V. Mineev, *Low Temp. Phys.* **37**, 872 (2011).  
 [9] D. Agterberg, in *Non-Centrosymmetric Superconductors* (Springer, New York, 2012), pp. 155–170.  
 [10] T. Ojanen, *Phys. Rev. Lett.* **109**, 226804 (2012).  
 [11] F. Konschelle, I. V. Tokatly, and F. S. Bergeret, *Phys. Rev. B* **92**, 125443 (2015).  
 [12] F. S. Bergeret and I. V. Tokatly, *Europhys. Lett.* **110**, 57005 (2015).  
 [13] K. Yasuda, H. Yasuda, T. Liang, R. Yoshimi, A. Tsukazaki, K. S. Takahashi, N. Nagaosa, M. Kawasaki, and Y. Tokura, *Nat. Commun.* **10**, 2734 (2019).  
 [14] R. Wakatsuki, Y. Saito, S. Hoshino, Y. M. Itahashi, T. Ideue, M. Ezawa, Y. Iwasa, and N. Nagaosa, *Sci. Adv.* **3**, e1602390 (2017).  
 [15] R. Wakatsuki and N. Nagaosa, *Phys. Rev. Lett.* **121**, 026601 (2018).  
 [16] F. Ando, Y. Miyasaka, T. Li, J. Ishizuka, T. Arakawa, Y. Shiota, T. Moriyama, Y. Yanase, and T. Ono, *Nature (London)* **584**, 373 (2020).  
 [17] C. Baumgartner, L. Fuchs, A. Costa, S. Reinhardt, S. Gronin, G. C. Gardner, T. Lindemann, M. J. Manfra, P. E. Faria Junior, D. Kochan *et al.*, *Nat. Nanotechnol.* **17**, 39 (2022).  
 [18] C. Baumgartner, L. Fuchs, A. Costa, J. P. Cortes, S. Reinhardt, S. Gronin, G. C. Gardner, T. Lindemann, M. J. Manfra, P. E. F. Junior *et al.*, *J. Phys. Condens. Matter* **34**, 154005 (2022).  
 [19] H. Wu, Y. Wang, P. K. Sivakumar, C. Pasco, S. S. Parkin, Y.-J. Zeng, T. McQueen, and M. N. Ali, *arXiv:2103.15809*.  
 [20] J. J. He, Y. Tanaka, and N. Nagaosa, *arXiv:2106.03575*.  
 [21] N. F. Yuan and L. Fu, *arXiv:2106.01909*.  
 [22] A. Daido, Y. Ikeda, and Y. Yanase, *Phys. Rev. Lett.* **128**, 037001 (2022).  
 [23] L. Bauriedl, C. Bäuml, L. Fuchs, C. Baumgartner, N. Paulik, J. M. Bauer, K.-Q. Lin, J. M. Lupton, T. Taniguchi, K. Watanabe *et al.*, *arXiv:2110.15752*.  
 [24] B. Zinkl, K. Hamamoto, and M. Sgrist, *arXiv:2111.05340*.  
 [25] F. Dolcini, M. Houzet, and J. S. Meyer, *Phys. Rev. B* **92**, 035428 (2015).  
 [26] M. Houzet and J. S. Meyer, *Phys. Rev. B* **92**, 014509 (2015).  
 [27] Note that by taking the ansatz  $\Delta(x) = \Delta e^{iqx}$  we made an important assumption—that the helical phase appears in the whole phase diagram, at any  $T$  and  $h$ . This is, however, not always true. Namely, at  $\alpha/v < 0.25$ , low  $T$  and sufficiently high  $h$ , the so-called stripe phase, characterized by multiple modulation vectors, can be stabilized instead of the helical phase [28,29]. Importantly, already at  $\alpha/v = 0.05$  the majority of the  $h-T$  phase diagram is occupied by the helical phase with a small region of stripe phase. This region reduces by increasing  $\alpha$ , until it disappears at  $\alpha/v = 0.25$  [29]. Disorder further suppresses the stripe phase. For these reasons, in this work we focus only on the helical phase, while neglecting the stripe phase. The effect this phase would have on the diode effect remains an interesting open question.  
 [28] O. Dimitrova and M. V. Feigel’man, *Phys. Rev. B* **76**, 014522 (2007).

- [29] D. F. Agterberg and R. P. Kaur, *Phys. Rev. B* **75**, 064511 (2007).
- [30] See Supplemental Material at <http://link.aps.org/supplemental/10.1103/PhysRevLett.128.177001> which contains analytical expressions for the Fermi surface averages that enter Eqs. (5) and (6) in the ballistic limit, technical details on solving the linearized Eilenberger equation (4), analytical demonstration that the diode effect vanishes close to  $T_c$  up to linear order in  $h$ , and analysis of the diode effect in a broad disorder range.
- [31] A. Hijano, S. Ilić, M. Rouco, C. González-Orellana, M. Ilyn, C. Rogero, P. Virtanen, T. T. Heikkilä, S. Khorshidian, M. Spies, N. Ligato, F. Giazotto, E. Strambini, and F. S. Bergeret, *Phys. Rev. Research* **3**, 023131 (2021).
- [32] E. Strambini, V. N. Golovach, G. De Simoni, J. S. Moodera, F. S. Bergeret, and F. Giazotto, *Phys. Rev. Mater.* **1**, 054402 (2017).
- [33] S. Manna, P. Wei, Y. Xie, K. T. Law, P. A. Lee, and J. S. Moodera, *Proc. Natl. Acad. Sci. U.S.A.* **117**, 8775 (2020).